Title	Defect chemistry and vacancy concentration of luminescent europium doped ceria nanoparticles by solvothermal method
Author(s)	Thorat, Atul V.; Ghoshal, Tandra; Carolan, Patrick B.; Holmes, Justin D.; Morris, Michael A.
Publication date	2014-04-28
Original citation	Thorat, A. V., Ghoshal, T., Carolan, P., Holmes, J. D. and Morris, M. A. (2014) 'Defect Chemistry and Vacancy Concentration of Luminescent Europium Doped Ceria Nanoparticles by the Solvothermal Method', The Journal of Physical Chemistry C, 118(20), pp. 10700-10710. doi: 10.1021/jp410213n
Type of publication	Article (peer-reviewed)
Link to publisher's version	https://pubs.acs.org/doi/10.1021/jp410213n http://dx.doi.org/10.1021/jp410213n Access to the full text of the published version may require a subscription.
Rights	© 2014 American Chemical Society. This document is the Accepted Manuscript version of a Published Work that appeared in final form in Journal of Physical Chemistry C , copyright © American Chemical Society after peer review and technical editing by the publisher. To access the final edited and published work see https://pubs.acs.org/doi/10.1021/jp410213n
Item downloaded from	http://hdl.handle.net/10468/6788

University College Cork, Ireland
Coláiste na hOllscoile Corcaigh

Defect Chemistry and Vacancy Concentration of Luminescent Europium Doped Ceria Nanoparticles by Solvothermal Method

Atul V. Thorat,[†,‡,§] Tandra Ghoshal,[†,‡,§] Patrick Carolan,[‡] Justin D. Holmes,[†,‡,§] and Michael A. Morris[*,†,‡,§]

[†]Materials research group, Department of Chemistry, University College Cork, Cork, Ireland

[‡]Tyndall National Institute, University College Cork, Cork, Ireland

[§]Centre for Research on Adaptive Nanostructures and Nanodevices (CRANN), Trinity College Dublin, Dublin, Ireland

[*] Corresponding Author: Prof. Michael A. Morris

E-mail: m.morris@ucc.ie

Tel: + 353 21 490 2180

Fax: +353 21 427 4097

ABSTRAT: Pure phase and europium doped ceria nanocrystals have been synthesized by a single step simple solvothermal process. Different spectroscopic, diffractive and microscopic techniques were used to determine the morphology, size, crystal structure and phase of all the samples. Electron energy loss spectroscopy (EELS) for elemental mapping confirmed that good solid solutions were formed and that the particles had a homogeneous distribution of europium. The defect chemistry was more complex than might be expected with the incorporation of each Eu^{3+} ion resulting in the production of an anion vacancy since the doping results in charge compensating (i.e. for Eu^{3+}) anion vacancies as well as vacancies due to oxygen removal from the crystallite surface. Variations in nanoparticles dimension and lattice parameters were measured as a function of dopant concentrations and their variations explained. The band gap of the samples could be tailored by the doping. The doped samples were found to be luminescent due to the substitution of Ce^{4+} ions in the cubic symmetric lattice by the dopant ions. The thermal stability of the fluorescence properties was also investigated.

Keywords: ceria, europium, defects, doping, EELS, luminescence.

1. INTRODUCTION

Nanostructures of rare-earth cerium oxide (CeO_2) have been widely investigated because of its multiple applications in areas such as catalysis,[1] an electrolyte for solid oxide fuel cells,[2] UV absorbent and UV filter materials,[3] oxygen gas sensors,[4] polishing materials,[5] optical devices[6] and biomedicine.[7] CeO_2 has unique properties such as high refractive index, optical transparency, high dielectric constant, lattice expansion, stability at high temperature and mechanical robustness. It's applications generally take advantage of the excellent redox properties and high oxygen storage capacity (OSC) of CeO_2. This redox chemistry is, in part, related to the similar energy of the 4f and 5d electronic states and a low potential energy barrier to electron exchange between them.[8] In principle, the different electron configurations possible can be determined by core and valence level spectroscopies.[9] The properties of CeO_2 are thought to be controlled by the nature of the oxygen vacancies because oxygen diffusion depends on the type, size, and concentration of those vacancies.[10] Therefore, numerous investigations have been conducted to study the Ce^{3+} and O vacancy defect sites in CeO_2 using techniques including x-ray photoelectron spectroscopy (XPS), x-ray diffraction (XRD), electron paramagnetic resonance (EPR), scanning tunnelling microscopy (STM), Raman spectroscopy and neutron scattering.

There have been numerous attempts to optimize the physiochemical properties of CeO_2 by inclusion of metallic cation dopants which can control the anion vacancy and Ce^{3+} cation concentrations.[11] Doping can improve the sintering properties of CeO_2, by stabilizing the CeO_2 surface area and crystallite size.[12] Doping with divalent and trivalent dopants leads to formation of oxygen vacancies, and modification of oxygen mobility and ionic conductivity.[13] Unsurprisingly, this is reflected in changing the redox properties and oxygen storage capacity of the CeO_2. CeO_2 is a potentially important material in optical and optoelectronic applications but exhibits weak emission characteristics that limit its performance.[14] Doping with lanthanide

cations such as europium (Eu) can enhance the visible emission of CeO_2 nanoparticles through an increase in the concentration of oxygen vacancies.[15, 16] Europium is a convenient dopant since the ionic radius of the trivalent europium[17] (0.1066 nm) is between that of Ce^{3+} (0.1143 nm) and Ce^{4+} (0.097 nm) and this allows for extensive solubility in the CeO_2 fluorite structure. The Eu^{3+}/Eu^{2+} redox pair has a potential of about 0.36 V and is expected to create and stabilize the oxygen vacancies for low Eu^{3+}/Ce atomic ratios.[18] This property promotes charge transfer from oxygen ions through the lattice oxide and provides the material with high oxygen ion conductivity.[19] If energy is transmitted from this charge transfer state to lanthanide ions characteristic emissions are expected to be observed.[20]

As the morphological properties of CeO_2, such as the particle size, shape and specific surface area, usually determine the performance, various synthetic methods, such as co-precipitation,[21, 22] microemulsion,[23] flow,[24] reverse precipitation,[23] sol–gel processes[25] and electrochemical routes,[26] have all been used to prepare ultrafine CeO_2 powder with controlled dimension. Several precipitants and surfactants have also been used to control the particle size and homogeneity such as ammonium hydroxide, urea and ammonium hydrogen carbonate. However, through all of the above methods, nanocrystalline CeO_2 is more difficult and inconvenient to obtain; calcination is usually necessary for the crystallization of amorphous samples and/or the removal of the surfactants. It is also difficult to synthesize highly uniform and well-dispersed nanocrystalline CeO_2 on the basis of the following reasons. Firstly, it is not easy to choose the appropriate precursor complexes and the crystalline temperatures for rare-earth oxides are relatively high. Second, the agglomeration of nanocrystals is very common because the nanocrystals tend to decrease the exposed surface to lower the surface energy.[27] Solvothermal methods[28, 29] that do not involve catalysts, surfactants or templates provides a more promising option for the large scale production of high purity nanoparticles as they are simple, fast and less expensive. Moreover, solvothermal method possesses advantages of being

single step, low temperature, controlled composition and morphology as well as being less sensitive to particulate aggregation and producing crystalline nanocrystals.

Interestingly, despite the wealth of work, in many cases, the understanding of the defect science in many systems is only poorly understood. The role of anion defects to charge compensate low valency cations in the CeO_2 lattice is accepted but the role of dopants and their effect on neighbouring cerium cations is less clear and this paper reveals an interesting relationship. Here, different concentrations of europium ions were successfully introduced into the cubic phase CeO_2 lattice using solvothermal techniques. In our previous work,[30] a detailed study was carried out to investigate the defect structure and dynamics of Eu doped ceria nanoparticles by using positron annihilation spectroscopy. Here, this work is extended to study the defect chemistry by different spectroscopic techniques and EELS was used to study the concentration and distribution of the dopant ions. Additionally, the morphological and structural evolution and optical properties were correlated as a function of concentrations of europium doping as well as with further annealing.

2. EXPERIMENTAL SECTION

Materials. Europium (III) nitrate pentahydrate [$Eu(NO_3)_3.5H_2O$, 99.999%], cerium (III) nitrate hexahydrate [$Ce(NO_3)_3.6H_2O$, 99.999%], anhydrous ethanol (≥99.9%), absolute ethanol (≥99.8%) and 28% aqueous ammonia were purchased by Sigma-Aldrich and used as received.

Synthesis of europium doped CeO₂ nanoparticles. For the solvothermal synthesis of the CeO_2 nanoparticles, a closed cylindrical Teflon lined stainless steel chamber with 45 ml capacity was used. 0.1 M (1.52 g) of $Ce(NO_3)_3.6H_2O$ and an appropriate amount of ammonia (1-2 g) were dissolved in 35 ml of anhydrous ethanol in a Teflon bottle. This mixture was stirred for 5 min to which was added different concentrations of $Eu(NO_3)_3.5H_2O$ (0.3-50 atom% relative to cerium). The solution was stirred for another 15 min with the formation of milky slurry. Subsequently, the closed Teflon chamber was transferred into a preheated oven

and was subjected to solvothermal treatment at 180 °C for 12 h. Yellow precipitates were collected, washed with deionized water and absolute ethanol several times by centrifugation, followed by drying at 50 °C in air overnight. Samples with varying concentrations of europium are represented as CEEUX, where X = 0, 0.2, 0.8, 1.5, 3.9, 7.6, 13.9, 19.2, 24.6 and 29.2 are the determined atom % of Eu.

Characterizations. Powder x-ray diffraction (XRD) patterns were recorded on a PANalytical MPD instrument using an Xcelerator detector and Cu Kα radiation source. Total reflectance x-ray fluorescence spectroscopy (TXRF) was performed to obtain the actual Ce:Eu atomic ratio of the samples using Bruker S2 Picofox instrument. Morphologies and sizes were studied by Transmission electron microscopy (TEM, JEOL JEM 2100) operated at a voltage of 200 kV. For TEM imaging, samples were dispersed in anhydrous ethanol by ultrasonication, coated on copper grids and dried. Elemental maps were obtained with a FEI Titan TEM equipped with a magnetic sector electron energy-loss spectrometer and an energy dispersive X ray detector. X-ray photoelectron spectroscopy (XPS) was carried out on a VSW Atomtech system (Al Kα radiation at 50 eV pass energy) instrument. For optical absorption measurements, powder samples were dispersed in ethanol and the absorption spectra were recorded with a spectrophotometer (Cary 50). Photoluminescence measurements were carried out at room temperature using 325 nm as the excitation wavelength with a luminescence spectrometer (Perkin Elmer LS 50 B).

3. RESULTS

Dopant ion concentration by TXRF. The presence and the actual concentrations of europium ions in the cerium oxide powder was confirmed by TXRF (see supporting information) and summarized in Table 1. In all samples, the actual incorporation of europium concentration was found to be lower than that added during synthesis. This is normal and is explained by lower solubility of the europium cations in basic conditions.

Structural characterization by XRD. Crystal structures of the as-prepared samples were determined from the XRD patterns shown in Figure 1a. XRD patterns exhibit x-ray diffraction peaks which can be indexed to a cubic fluorite phase (JCPDS no. 04-0593) of ceria. The strongest XRD peak for all the samples was ascribable to the (111) plane of cubic CeO_2. The relative peak intensity of the remaining lattice planes varied with the change in doping concentrations. The existence of higher order features indicates good solid solutions were formed throughout the composition range. The broad nature of the peaks reveals the nanocrystalline nature of the samples. The patterns did not show any extra peaks, indicating that the samples are good solid solutions and there is no secondary phase indicative of europium oxides. The crystallite size was estimated from XRD peak broadening using the Scherrer equation,

$$d = \frac{0.9\lambda}{\beta \cos \theta}$$
Eq. 1

where d is the crystallite size, λ is the wavelength of Cu Kα radiation, β is the full-width at half maximum (FWHM) of the diffraction peak and θ is the diffraction angle. Figure 1b(i) shows the variation of crystallite size with doping concentrations. A sharp decrease in the crystallite size was observed with increasing the doping concentration up to 7.6 % and becomes almost constant with further doping. The decrease in crystallite size suggests that the dopant introduces significant lattice strain (the ionic radius of Eu^{3+} (0.107 nm) is about 10 % larger than that of Ce^{4+} (0.097 nm)[31]) and this reduces ion transport and sintering as noted previously for doped CeO_2.[32] The measured lattice parameter of undoped CeO_2 was found to be 0.542 nm somewhat higher than that reported for bulk CeO_2 (0.541 nm) but may be due to lattice expansion due to the presence of anion vacancies resulting from the preparation.[23] Figure 1b(ii) shows the variation of lattice parameters with doping concentrations. An initial decrease in the lattice parameter was observed with increase in europium doping up to 1.5 % but increases upon further doping. The expansion of the lattice with increasing dopant concentration is

consistent with the substitution of the smaller Ce^{4+} ions by the larger Eu^{3+} ions. Similar trend was reported due to incorporation of another trivalent dopant Gd^{3+} in ceria as the ionic radius of Gd^{3+} is 0.1053 nm, higher than that of Ce^{4+} ions.[33, 34] The increase in lattice parameter is mirrored by the decrease in crystallite size almost exactly confirming the relationship of these two effects. The relationship of both parameters is not linearly dependent on the dopant concentration but, rather, tends towards a limiting value. This is not consistent with a random substitution of CeO_2 cations with europium cations and suggests this is at least a locally ordered arrangement. The small but reproducible decrease in the lattice parameter at low dopant concentrations is consistent with a surface-tension type effect at very small crystallite sizes as discussed by us previously.[23] It is asserted that as the crystallite size decreases very rapidly at low dopant concentration, the lattice contraction due to surface tension exceeds the small expansion due to europium addition. Indeed, the measured strain does appear to increase with europium loading as shown in Table 2. Table 2 summarizes the variation of crystallite size, lattice parameters and lattice strains with europium concentrations.

The as-synthesized samples were annealed at different temperatures to study structural evolution. Figure 1c shows illustrative XRD patterns of CEEU7.6 annealed at different temperatures. As above, only the fluorite structure was present in all scans suggesting good solid solutions were formed at all temperatures. The existence of small amounts of europium could be dispersed at the surface of CeO_2. The XRD reflections peak widths and the background signal reduce as the calcination temperature is increased consistent with grain coarsening. Table 2 summarizes the variation of crystallite size, lattice parameters and lattice strains for sample CEEU7.6 annealed at different temperatures.

Composition and Oxidation state determination by XPS. XPS was used to study composition and valence states of the undoped and doped samples. The recorded XPS spectra were charge-corrected with respect to an adventitious C 1s signal at 285 eV. Representative

survey spectra of the CEEU0 and CEEU7.6 samples reveal the presence of cerium, oxygen and carbon as well as europium for the doped samples (Figure 2a). There is a significant carbon content which is typical of adventitious carbon arising from atmospheric exposure. No other significant contamination was detected. The Ce3d photoelectron spectra of cerium compounds can be used to identify cerium valence states but the spectra are complicated because of final state effects involving hybridization of the Ce4f orbitals with O2p orbitals and fractional occupancy of the valence 4f orbitals.[35] Because of these effects, electron transfer from O2p to Ce4f orbitals can occur during photoemission giving rise to the appearance of multiple oxidation states. Thus, the Ce $3d_{5/2}$ photoelectron spectrum has three principle features (for each spin-orbit doublet) in the case of CeO_2 and two for Ce_2O_3.[36] In this way, a mixed valence sample can contain ten peaks altogether for overlapping Ce $3d_{5/2}$ and Ce $3d_{3/2}$ spin-orbit bands.[37] These peaks are usually described by nomenclature developed by Burroughs et al.[38] U, $U^{//}$, $U^{///}$ and V, $V^{//}$, $V^{///}$ (note states labelled U or V refer to $3d_{3/2}$ and $3d_{5/2}$ respectively) are characteristic of Ce(IV)3d final states; while U_0, $U^{/}$ and V_0, $V^{/}$ refer to Ce(III) 3d final states. The high binding energy doublet $V^{///}/U^{///}$ at 898.2 eV and 916.4 eV are assigned to a Ce(IV) final state of $3d^94f^0O2p^6$. Doublets $V^{//}/U^{//}$ at 888.4 eV and 907.6 eV were attributed to the hybridization state of Ce(IV)$3d^94f^1O2p^5$, and doublets V/U at 882.3 eV and 901.1 eV correspond to the state of Ce(IV)$3d^94f^2O2p^4$. Doublets $V^{/}/U^{/}$ and V_0/U_0 are due to a mixture of Ce(III)$3d^94f^2O2p^4$ and Ce(III)$3d^94f^1O2p^5$ configurations at 886 eV, 904.6 eV and 880.3 eV, 899.2 eV respectively.[39] By comparison to previous work it can be concluded that the Ce3d spectrum for the undoped sample indicates it is essentially a stoichiometric CeO_2 structure (Figure 2b). The Ce3d photoelectron spectra for the doped samples exhibits features which can be assigned to the presence of Ce(III) states (Figure 2b). Most obvious is an increased intensity at around 886 eV and 904 eV (marked with arrows in Figure 2b) and a reduction in relative peak intensity for the feature around 918 eV. It is clear that these contributions increase with

dopant concentration. Figure 2c is curve-fitted data for the Ce3d spectrum of sample CEEU7.6 and is consistent with a mixed valence CeO_2 material. Other materials gave similar data. Curve-fitting of the spectra from the samples allows quantification of the atomic% of Ce(III)[40] using Equation 2 and is summarized in Table 2 for all the samples.

$$[Ce^{3+}] = \frac{U_0 + U' + V_0 + V'}{U_0 + U' + V_0 + V' + U + U'' + U''' + V + V'' + V'''}$$

Eq. 2

From the data provided in Table 2, it is seen that the concentration of Ce^{3+} increases linearly with europium addition. Indeed, if the actual europium concentration is compared to the measured Ce^{3+} concentration, it can be seen that around one Ce^{3+} cation is created for every Eu^{3+} addition through the formation of oxygen vacancy ($V_0^{\bullet\bullet}$). This is somewhat unexpected. Indeed, according to results gathered in Table 2, highest Ce^{3+} contents are found for highest strain values.

Using Kröger–Vink notation the generally accepted mechanism for dissolution of a trivalent lanthanide oxide such as europium oxide into ceria can be described by the equation:

$$Eu_2O_3 + 2Ce^x{}_{Ce} + O_O^x \rightarrow 2Eu'_{Ce} + V_O^{\bullet\bullet} + 2CeO_2$$

Eq. 3

where, Eu'_{Ce} signifies a dopant substitution (of a cerium cation) and $V_0^{\bullet\bullet}$ an oxygen vacancy. In this way, each Eu ion dopant replaces host cations (Ce^{4+}) by Eu^{3+} and for every two Eu^{3+} and extends the lattice. The substitution also results in the formation of an oxygen vacancy to satisfy charge neutrality. Note, that having an effective charge of opposite signs, oxygen vacancies and trivalent dopants can attract each other. Chemically, this vacancy mechanism can be represented $CeO_2 + x/2Eu_2O_3 \rightarrow Ce_{1-x}Eu_xO_{2-x/2}$ where the resultant solid solution has a structure similar to that of fluorite (CeO_2) apart from a distribution of anion vanacies. However, this does not reflect the formation of Ce^{3+} cations observed here and a more reasonable representation is given by:

$$Eu_2O_3 + 2Ce^x{}_{Ce} \rightarrow 2Ce'_{Ce} + 2Eu'_{Ce} + 2V_O^{\bullet\bullet} + 2O_O^x + 1/2O_2$$

Eq. 4
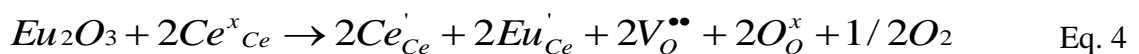
This shows that trivalent europium cation is accompanied by the production of a cerium trivalent cation (plus an additional vacancy for each of these and gas phase oxygen). In simple chemical terms the solid state solution can be written stoichiometrically as $Ce_{1-x}Eu_xO_{2-x}$. This implies that there is additional thermodynamic stability of defect clusters such as Eu^{3+}-V_o-Ce^{3+} compared to Eu^{3+}-V_o-Ce^{4+}. Note that these are simple representations of what will actually be 3D structural arrangements and are used for brevity here. The existence of this kind of defect clustering was reported for large to small (La or Lu) dopant incorporation into the ceria lattice in order to achieve electrostatic stabilization of the crystal.[41, 42] This kind of vacancy agglomeration was also observed by us before[30] which increases with increasing the dopant concentration. This higher content of vacancies at the surface for highly doped samples might decrease the reducibility of the compounds in order to preserve the equilibrium of reaction. This is evident from Table II which depicts the rate of formation of Ce^{3+} decreases with higher doping concentrations as proposed for Gd^{3+} dopant.[33] Recent work by Nolan et al[43] suggest that O^- species may also be stable in doped CeO_2 fluorite structures although there is no direct evidence for this mechanism here.

Ceria-based nanopowders, are important for their surface redox capabilities and their general catalytic activity.[44] Their surface redox capability possibly incorporates switching between Ce^{4+} and Ce^{3+} oxidation states through an ability to absorb and release oxygen by generating oxygen vacancies in the ceria lattice. The experiment was performed in a closed solvothermal chamber for which it can be considered that the concentration of oxygen in the atmosphere around the sample is orders of magnitude lower than the concentration of oxygen at the surfaces of CeO_2 particles.[45] This gradient of concentration might be the driving force for the oxygen removal from the surface of the particle which reduces Ce^{4+} into Ce^{3+}.

The possibility of oxidizing some of the Ce^{3+} ions to Ce^{4+} at higher temperatures is revealed in Figure 2d which shows the Ce3d spectra of the CEEU7.6 sample annealed at 500 °C, 700

°C and 900 °C for 2 h. These data are also indicative of mixed Ce(III) and Ce(IV) valence states but at reduced concentration compared to the non-calcined form suggesting that the system has a well-defined redox chemistry. Table 2 describes that the concentrations of Ce^{3+} ions decreases with the increase in annealing temperature. It is suggested that some of the surface oxygen vacancies were oxidized by the high temperature exposure to atmospheric oxygen which transforms Ce^{3+} ions into Ce^{4+} ions. The particle sizes also increases with the increases in annealing temperature through particle agglomeration. Thus, the annealing step results an increase in particle sizes and changes in oxidation state.

The valence state of europium is confirmed by Eu3d XPS spectrum. All samples gave similar spectra and representative Eu3d data are shown in Figure 2b (inset) for sample CEEU7.6. The two characteristic peaks at 1134 ($3d_{5/2}$) and 1163 eV ($3d_{3/2}$) correspond to the Eu^{3+} state. Previous work has shown that the binding energy shift of Eu3d features for Eu^{3+} and Eu^{2+} are around 10 eV[46] and this assignment is rather clear.

Morphological and compositional studies by TEM. TEM images of the undoped and doped CeO_2 samples confirm the nanocrystalline nature of the samples. Figure 3a, b, c and d represent TEM micrographs for the CEEU0, CEEU0.8, CEEU7.6 and CEEU19.2 samples. There was no obvious particulate morphology change and all the samples were composed of small agglomerated crystallites with an irregular pseudo-spherical shape of uniform size distribution and a diameter between 5 to 10 nm, similar to that estimated from XRD. The mean diameters measured confirm a size decrease with increased europium concentration. Clearly visible lattice fringes suggest a high degree of crystallinity of the particles for all the samples. Analysis suggests the facets are (111) planes consistent with other work and known stabilities.[47, 48] The measured interplanar distance is 0.32 nm corresponds to the (111) plane of fluorite cubic structure of CeO_2. The SAED patterns shown in the inset of Figure 3 also indicate

high degrees of crystallinity and are consistent with (111), (220) and (311) reflections from a fluorite phase.

A highlight of this work was the use of high spatial EELS to demonstrate the location of Eu in these materials and confirm solid state solution. Figure 4a and b shows the dark field TEM image and Ce L_α, Eu L_α, O K_α elemental mapping of a nanoparticle of 4.5 nm in diameter for the sample CEEU7.6 and CEEU19.2 respectively. The image (red square box) represents the CeO_2 nanoparticle which provides a reference to locate the area of the elemental map. The mapping was obtained as a pixel-by-pixel mapping of the integrated intensity of the EELS spectrum. The spectrum taken from few of the nanoparticles in different area was essentially the same. The elemental maps confirm the presence of Eu, Ce and O throughout the nanoparticle.[22, 49] This results indicate that the Eu incorporation inside the ceria nanocrystal and not present as a free species within the powdered sample and suggest little surface segregation etc. Corresponding EDX spectrum also confirms an increase in the intensity of the Eu peak with the increment of doping concentrations.

Optical properties. Absorption spectra of nanomaterials can provide useful analysis of nanophase oxide materials. Figure 5 shows the UV-Visible spectra of undoped and europium doped CeO_2 nanoparticles. It can be seen that the absorbance peaks shifts towards higher wavelength (red-shift) with the increasing europium content, characteristic of electron-phonon coupling phenomenon[50] and decreasing nanocrystallite sizes increase electron-phonon-coupling coefficients. These effects derive from changes in the band structure with reduced dimension which modify the effective mass/mobility and lattice scattering of the carriers and result in a red-shift of the emission band.[51] Theoretically, absorbance band edge shifts towards the shorter wavelength is demonstrated as a blue-shift. The size of the particle is readily influenced by the quantum confinement consequences. It is well known that decreasing size of materials increases with the electron-phonon-coupling coefficients. In certain systems,

electron-phonon coupling could be strong enough to overcome the spatial confinement to determine the energy of excitons. It determines or modifies the effective mass of carriers and the style of carrier scattering by the lattice, leading to a red-shift of the emission band. It has also been suggested that the red-shift of the absorption bands observed in nanocrystalline CeO_2 can be explained by the formation of localized states within the band gap owing to oxygen vacancies and an increase of the Ce^{3+} ion concentration.[52, 53] This phenomenon is related to the shift of absorbance band towards longer wavelength. Chowdhury et. al. and other authors reported the similar red shift in wavelength with the increase in Ce^{3+} concentration.[52-54] The band gap of undoped and europium doped CeO_2 samples are calculated from UV-Vis spectra and listed in Table 2.

Photoluminescence (PL) spectroscopy is an effective method to determine the optical properties of materials and the defect chemistry associated with those properties.[31, 55] Figure 6a shows the excitation spectra for emission at 608 nm of undoped and europium doped CeO_2 samples. CEEU0 does not show any emission peak around the excitation energy but well-defined features around 466 nm characteristic of europium 4f-4f transitions[56] were observed in all europium doped samples. Because the O^{2-}-Eu^{3+} charge transfer lies at much shorter wavelengths and CeO_2 has a band gap around 3.3 eV (~470 nm), the broad peak is related to mainly Ce^{4+}-O^{2-} charge transfer[57] with some overlap with the intraconfigurational Eu 4f-4f transitions. As evident from Figure 6a, with increasing europium content the intra $4f^6$ transition bands of Eu^{3+} become generally stronger to a maximum of 19.2 % beyond which the intensity decreases due to a concentration quenching effect.[58] Figure 6b describes the excitation spectra of CEEU7.6 with different annealing temperatures. The intensity of the peak at 466 nm increases with the annealing temperature because Ce^{4+}-O^{2-} charge transfer becomes predominant due to the formation of more Ce^{4+}.

Figure 7a, b shows the emission spectra of various europium doped and annealed CeO_2 samples for excitation at 466 nm. As seen in the higher wavelength excitation, with increasing Eu^{3+} concentration, there is an increase in intensity up to 19.2 % a further increase in dopant concentration decreases the Eu^{3+}-Eu^{3+} distance, indicating an effective energy transfer between the neighbouring ions. Hence, the excited state is quenched, scattering the energy non-radiatively and the emission intensity decreases. The emission spectra reveal a characteristic Eu^{3+} emission and can be assigned to various transitions $^5D_0$-^7F_J (J=0, 1, 2 etc.) that reveal the local environment of the Eu^{3+} ion. The multiple peaks in the spectra are due to the splitting of the Eu^{3+} 4f shell. The Judd-Ofelt (J-O)[59, 60] theory is the most useful method in the analysis of spectroscopic studies of lanthanide ions in different hosts. As per J-O theory, the emission lines are a cumulative effect of magnetic dipole (MD) transition and electric dipole (ED) transition, depending on the specific environment of Eu^{3+} in any matrix. According to the J-O theory, the ED transition (^5D_o-$^7F_2$) centered at about 611 and 629 nm, is only allowed in the absence of inversion symmetry and is hypersensitive to the local electric field. On the other hand, the MD transition (^5D_o-$^7F_1$) with emission at 591 nm is a magnetic dipole allowed transition, which is insensitive to the crystal environment. CeO_2 has a cubic fluorite structure with every Ce ion surrounded by eight equatorial oxygen ions in O_h symmetry. The emission intensity of Eu^{3+} is very critical to its location in the lattice, that is, the type of environment around Eu^{3+} ions. When Ce^{4+} is replaced with Eu^{3+}, the symmetry can be lowered or increased depending on the site occupied by the dopant. In the present case, the ED transition intensity was found to be higher, indicating that Eu^{3+} mainly occupies the lattice sites. The absence of any forbidden electric or magnetic dipole transitions also indicates a high symmetry Eu site suggesting simple substitution with fluorite Ce^{4+} sites.

The emission intensity was found to increase with the increase in annealing temperature (Figure 7b). The temperature insensitivity of the form of the PL emission peaks confirms that

Eu^{3+} ions occupy fluorite structure cation sites substitutionally at all temperatures. The similarity in the data also demonstrates that the interaction between the europium-dopant and oxygen vacancy resulting from charge compensation Eu^{3+}–Ce^{4+} is neither enhanced nor diminished with the increasing temperature. However, the increase in intensity and narrowing of peaks is due to the more crystalline-like environment obtained at higher calcinations.

4. CONCLUSIONS

In summary, europium doped CeO$_2$ nanoparticles have been successfully synthesized by a single step simple solvothermal process. The as-formed nanoparticles are highly crystalline and their sizes varied in the range of 3-9 nm depending on the europium concentrations. An increase in the measured lattice parameter was observed due to inclusion of the larger europium cations but at very small doping concentrations, lattice contraction was observed due to surface tension-type effects. The europium ion site occupancy through the substitution of Ce^{4+} ions in the cubic symmetric lattice was verified and found to be less compared to the dopant ion added during synthesis. The insertion of the rare earth cations in the CeO$_2$ structure provokes an increase in the oxygen vacancies concentration through the promotion of the non-stoichiometric condition of the cerium oxide, by the reduction of Ce^{4+} to Ce^{3+}. The crystal structure and spectroscopic analysis reveals almost similar concentrations for Ce^{3+} and Eu^{3+} suggest the europium species are mainly located in the lattice sites. The incorporation and homogeneous distribution of europium ions in the ceria nanoparticle is also confirmed. The band gap of the doped CeO$_2$ nanocrystals were found to decrease with the doping due to the formation of localized states within the band gap owing to the increase in oxygen vacancies and Ce^{3+} concentrations. The PL spectra indicate the high symmetry europium ions substitution with Ce^{4+} which is not affected with the calcinations temperature. The high temperature calcinations reduce the defect density, increasing the crystallite size thereby increasing the degree of crystallization. The ability to tailor the ionization state of cerium and the oxygen

vacancy concentration in CeO_2 has applications in a broad range of fields, which include catalysis, biomedicine, electronics, and environmental sensing.

ASSOCIATED CONTENT

Supporting Information

Typical TXRF graphs, particle size distribution calculated from TEM and mapping of ceria by STEM. This material is available free of charge via the Internet at http://pubs.acs.org.

5. REFERENCES:

(1)   Bera, P.; Gayen, A.; Hegde, M. S.; Lalla, N. P.; Spadaro, L.; Frusteri, F.; Arena, F., Promoting Effect of CeO_2 in Combustion Synthesized Pt/CeO_2 Catalyst for CO Oxidation. *J. Phys. Chem. B* **2003,** *107,* 6122-6130.

(2)   Mogensen, M.; Sammes, N. M.; Tompsett, G. A., Physical, chemical and electrochemical properties of pure and doped ceria. *Solid State Ionics* **2000,** *129,* 63-94.

(3)   Li, R.; Yabe, S.; Yamashita, M.; Momose, S.; Yoshida, S.; Yin, S.; Sato, T., Synthesis and UV-shielding properties of ZnO- and CaO-doped CeO_2 via soft solution chemical process. *Solid State Ionics* **2002,** *151,* 235-241.

(4)   Bene, R.; Perczel, I. V.; Réti, F.; Meyer, F. A.; Fleisher, M.; Meixner, H., Chemical reactions in the detection of acetone and NO by a CeO_2 thin film. *Sens. Actuators B* **2000,** *71,* 36-41.

(5)   Treichel, H.; Frausto, R.; Srivatsan, S.; Whithers, B.; Meyer, T.; Morishige, R., Process optimization of dielectrics chemical mechanical planarization processes for ultralarge scale integration multilevel metallization. *J. Vac. Sci. Technol., A* **1999,** *17,* 1160-1167.

(6)   Goubin, F.; Rocquefelte, X.; Whangbo, M.-H.; Montardi, Y.; Brec, R.; Jobic, S., Experimental and Theoretical Characterization of the Optical Properties of CeO_2, $SrCeO_3$, and Sr_2CeO_4 Containing Ce^{4+} (f^0) Ions. *Chem. Mater.* **2004,** *16,* 662-669.

(7)   Chen, J. P.; Patil, S.; Seal, S.; McGinnis, J. F., Rare earth nanoparticles prevent retinal degeneration induced by intracellular peroxides. *Nat. Nanotechnol.* **2006,** *1,* 142-150.

(8)   Macedo, A.; Fernandes, S. E.; Valente, A.; Ferreira, R. A.; Carlos, L.; Rocha, J., Catalytic Performance of Ceria Nanorods in Liquid-Phase Oxidations of Hydrocarbons with tert-Butyl Hydroperoxide. *Molecules* **2010,** *15,* 747-765.

(9)   Hufner, S., Screening in the Valence-Band Photoemission Spectra of Light Rare-Earths. *J. Phys. F: Met. Phys.* **1986,** *16,* L31-L34.

(10)   Dutta, P.; Pal, S.; Seehra, M. S.; Shi, Y.; Eyring, E. M.; Ernst, R. D., Concentration of Ce^{3+} and oxygen vacancies in cerium oxide nanoparticles. *Chem. Mater.* **2006,** *18,* 5144-5146.

(11)   Etsell, T. H.; Flengas, S. N., Electrical properties of solid oxide electrolytes. *Chem. Rev.* **1970,** *70,* 339-376.

(12)   Trovarelli, A., Catalytic Properties of Ceria and CeO_2-Containing Materials. *Catal. Rev.* **1996,** *38,* 439-520.

(13)   Inaba, H.; Tagawa, H., Ceria-based solid electrolytes. *Solid State Ionics* **1996,** *83,* 1-16.

(14) Mialon, G.; Poggi, M.; Casanova, D.; Nguyen, T. L.; Turkcan, S.; Alexandrou, A.; Gacoin, T.; Boilot, J. P., Luminescent oxide nanoparticles with enhanced optical properties. *J. Lumin.* **2009,** *129,* 1706-1710.

(15) Wang, X.; Hanson, J. C.; Liu, G.; Rodriguez, J. A.; Iglesias-Juez, A.; Fernández-García, M., The behavior of mixed-metal oxides: Physical and chemical properties of bulk $Ce_{1-x}Tb_xO_2$ and nanoparticles of $Ce_{1-x}Tb_xO_y$. *J. Chem. Phy.* **2004,** *121,* 5434-5444.

(16) Borchert, H.; Frolova, Y. V.; Kaichev, V. V.; Prosvirin, I. P.; Alikina, G. M.; Lukashevich, A. I.; Zaikovskii, V. I.; Moroz, E. M.; Trukhan, S. N.; Ivanov, V. P.; Paukshtis, E. A.; Bukhtiyarov, V. I.; Sadykov, V. A., Electronic and chemical properties of nanostructured cerium dioxide doped with praseodymium. *J. Phys. Chem. B* **2005,** *109,* 5728-5738.

(17) Shannon, R., Revised effective ionic radii and systematic studies of interatomic distances in halides and chalcogenides. *Acta Crystallogr., Sect. A* **1976,** *32,* 751-767.

(18) Tiseanu, C.; Parvulescu, V. I.; Boutonnet, M.; Cojocaru, B.; Primus, P. A.; Teodorescu, C. M.; Solans, C.; Dominguez, M. S., Surface versus volume effects in luminescent ceria nanocrystals synthesized by an oil-in-water microemulsion method. *Phys. Chem. Chem. Phys.* **2011,** *13,* 17135-17145.

(19) Yokokawa, H.; Horita, T.; Sakai, N.; Yamaji, K.; Brito, M. E.; Xiong, Y. P.; Kishimoto, H., Ceria: Relation among thermodynamic, electronic hole and proton properties. *Solid State Ionics* **2006,** *177,* 1705-1714.

(20) Fujihara, S.; Oikawa, M., Structure and luminescent properties of CeO_2:rare earth (RE=Eu^{3+} and Sm^{3+}) thin films. *J. Appl. Phys.* **2004,** *95,* 8002-8006.

(21) Djuričić, B.; Pickering, S., Nanostructured cerium oxide: preparation and properties of weakly-agglomerated powders. *J. Eur. Ceram. Soc.* **1999,** *19,* 1925-1934.

(22) Sun, C.; Li, H.; Chen, L., Nanostructured ceria-based materials: synthesis, properties, and applications. *Energy & Environ. Sci.* **2012,** *5,* 8475-8505.

(23) Chen, L.; Fleming, P.; Morris, V.; Holmes, J. D.; Morris, M. A., Size-Related Lattice Parameter Changes and Surface Defects in Ceria Nanocrystals. *J. Phys. Chem. C* **2010,** *114,* 12909-12919.

(24) Bondioli, F.; Corradi, A. B.; Manfredini, T.; Leonelli, C.; Bertoncello, R., Nonconventional Synthesis of Praseodymium-Doped Ceria by Flux Method. *Chem. Mater.* **1999,** *12,* 324-330.

(25) Ksapabutr, B.; Gulari, E.; Wongkasemjit, S., Sol–gel derived porous ceria powders using cerium glycolate complex as precursor. *Mater. Chem. Phys.* **2006,** *99,* 318-324.

(26) Zhou, Y.; Phillips, R. J.; Switzer, J. A., Electrochemical Synthesis and Sintering of Nanocrystalline Cerium(IV) Oxide Powders. *J. Am. Ceram. Soc.* **1995,** *78,* 981-985.

(27) Wang, Z.; Quan, Z.; Lin, J., Remarkable Changes in the Optical Properties of CeO_2 Nanocrystals Induced by Lanthanide Ions Doping. *Inorg. Chem.* **2007,** *46,* 5237-5242.

(28) Chengyun, W.; Yitai, Q.; Xie, Y.; Changsui, W.; Yang, L.; Guiwen, Z., A novel method to prepare nanocrystalline (7 nm) ceria. *Mater. Sci. Eng., B* **1996,** *39,* 160-162.

(29) Wang, Z. L.; Feng, X., Polyhedral Shapes of CeO_2 Nanoparticles. *J. Phys. Chem. B* **2003,** *107,* 13563-13566.

(30) Thorat, A. V.; Ghoshal, T.; Holmes, J. D.; Nambissan, P. M.; Morris, M. A., A positron annihilation spectroscopic investigation of europium-doped cerium oxide nanoparticles. *Nanoscale* **2013,** *6,* 608-615.

(31) Kumar, A.; Babu, S.; Karakoti, A. S.; Schulte, A.; Seal, S., Luminescence Properties of Europium-Doped Cerium Oxide Nanoparticles: Role of Vacancy and Oxidation States. *Langmuir* **2009,** *25,* 10998-11007.

(32) Ryan, K. M.; McGrath, J. P.; Farrell, R. A.; O'Neill, W. M.; Barnes, C. J.; Morris, M. A., Measurements of the lattice constant of ceria when doped with lanthana and praseodymia

- the possibility of local defect ordering and the observation of extensive phase separation. *J. Phys.: Condens. Matter* **2003,** *15,* L49-L58.

(33) Suresh, B.; Ranjith, T.; Talgat, I.; Richard, D.; Artëm, E. M.; Alfons, S.; Sudipta, S., Dopant-mediated oxygen vacancy tuning in ceria nanoparticles. *Nanotechnology* **2009,** *20,* 085713.

(34) Le Gal, A.; Abanades, S., Dopant Incorporation in Ceria for Enhanced Water-Splitting Activity during Solar Thermochemical Hydrogen Generation. *J. Phys. Chem. C* **2012,** *116,* 13516-13523.

(35) Liu, G.; Rodriguez, J. A.; Hrbek, J.; Dvorak, J.; Peden, C. H. F., Electronic and Chemical Properties of $Ce_{0.8}Zr_{0.2}O_2(111)$ Surfaces: Photoemission, XANES, Density-Functional, and NO_2 Adsorption Studies. *J. Phys. Chem. B* **2001,** *105,* 7762-7770.

(36) Park, P. W.; Ledford, J. S., Effect of Crystallinity on the Photoreduction of Cerium Oxide: A Study of CeO_2 and Ce/Al_2O_3 Catalysts. *Langmuir* **1996,** *12,* 1794-1799.

(37) Romeo, M.; Bak, K.; El Fallah, J.; Le Normand, F.; Hilaire, L., XPS Study of the reduction of cerium dioxide. *Surf. Interface Anal.* **1993,** *20,* 508-512.

(38) Burroughs, P.; Hamnett, A.; Orchard, A. F.; Thornton, G., Satellite structure in the X-ray photoelectron spectra of some binary and mixed oxides of lanthanum and cerium. *J. Chem. Soc., Dalton Trans.* **1976,** 1686-1698.

(39) Ghoshal, T.; Fleming, P. G.; Holmes, J. D.; Morris, M. A., The stability of "Ce_2O_3" nanodots in ambient conditions: a study using block copolymer templated structures. *J. Mater. Chem.* **2012,** *22,* 22949-22957.

(40) Deshpande, S.; Patil, S.; Kuchibhatla, S. V. N. T.; Seal, S., Size dependency variation in lattice parameter and valency states in nanocrystalline cerium oxide. *Appl. Phys. Lett.* **2005,** *87,* 133113.

(41)   Andersson, D. A.; Simak, S. I.; Skorodumova, N. V.; Abrikosov, I. A.; Johansson, B., Optimization of ionic conductivity in doped ceria. *Proc. Natl. Acad. Sci. U. S. A.* **2006,** *103,* 3518-3521.

(42)   Frayret, C.; Villesuzanne, A.; Pouchard, M.; Mauvy, F.; Bassat, J. M.; Grenier, J. C., Identifying Doping Strategies To Optimize the Oxide Ion Conductivity in Ceria-Based Materials. *J. Phys. Chem. C* **2010,** *114,* 19062-19076.

(43)   Yeriskin, I.; Nolan, M., Doping of ceria surfaces with lanthanum: a DFT + U study. *J. Phys. Condens. Matter.* **2010,** *22,* 135004.

(44)   Chen, M. Y.; Zu, X. T.; Xiang, X.; Zhang, H. L., Effects of ion irradiation and annealing on optical and structural properties of CeO_2 films on sapphire. *Physica B* **2007,** *389,* 263-268.

(45)   Stan, M.; Zhu, Y. T.; Jiang, H.; Butt, D. P., Kinetics of oxygen removal from ceria. *J. Appl. Phys.* **2004,** *95,* 3358-3361.

(46)   Cho, E. J.; Oh, S. J., Surface valence transition in trivalent Eu insulating compounds observed by photoelectron spectroscopy. *Phys. Rev. B* **1999,** *59,* R15613-R15616.

(47)   Sayle, T. X. T.; Parker, S. C.; Catlow, C. R. A., The role of oxygen vacancies on ceria surfaces in the oxidation of carbon monoxide. *Surf. Sci.* **1994,** *316,* 329-336.

(48)   Barnard, A. S.; Kirkland, A. I., Combining Theory and Experiment in Determining the Surface Chemistry of Nanocrystals. *Chem. Mater.* **2008,** *20,* 5460-5463.

(49)   Turner, S.; Lazar, S.; Freitag, B.; Egoavil, R.; Verbeeck, J.; Put, S.; Strauven, Y.; Van Tendeloo, G., High resolution mapping of surface reduction in ceria nanoparticles. *Nanoscale* **2011,** *3,* 3385-3390.

(50)   Zhang, Y.; Cheng, T.; Hu, Q.; Fang, Z.; Han, K., Study of the preparation and properties of CeO_2 single/multiwall hollow microspheres. *J. Mater. Res.* **2007,** *22,* 1472-1478.

(51)   Zhou, B.; Liangzhi, X.; Li, T.; Zhao, J.; Lai, Z.; Gu, S., Absorption redshift in TiO_2 ultrafine particles with surfacial dipole layer. *Appl. Phys. Lett.* **1991,** *59,* 1826-1828.

(52) Lu, X.; Li, X.; Chen, F.; Ni, C.; Chen, Z., Hydrothermal synthesis of prism-like mesocrystal CeO_2. *J. Alloys Compd.* **2009,** *476,* 958-962.

(53) Charitidis, C. P., P.; Logothetidis, S., Optical and mechanical performance of nanostructured cerium oxides for applications in optical devices. *J. Phys. Conf. Ser.* **2005,** *10,* 226-229.

(54) Lin, K. S.; Chowdhury, S., Synthesis, characterization, and application of 1-d cerium oxide nanomaterials: a review. *Int. J. Mol. Sci.* **2010,** *11,* 3226-51.

(55) Tiseanu, C.; Parvulescu, V. I.; Boutonnet, M.; Cojocaru, B.; Primus, P. A.; Teodorescu, C. M.; Solans, C.; Sanchez-Dominguez, M., Surface versus volume effects in luminescent ceria nanocrystals synthesized by an oil-in-water microemulsion method (vol 13, pg 17135, 2011). *Phys. Chem. Chem. Phys.* **2011,** *13,* 21652-21653.

(56) Hemmilä, I.; Mukkala, V.-M.; Takalo, H., Development of luminescent lanthanide chelate labels for diagnostic assays. *J. Alloys Compd.* **1997,** *249,* 158-162.

(57) Li, L.; Zhou, S.; Zhang, S., Investigation on charge transfer bands of Ce^{4+} in Sr_2CeO_4 blue phosphor. *Chem. Phys. Lett.* **2008,** *453,* 283-289.

(58) Juan, L.; Makoto, K., Preparation and luminescent properties of Eu-doped $BaTiO_3$ thin films by sol–gel process. *Sci. Technol. Adv. Mater.* **2003,** *4,* 143.

(59) Judd, B. R., Optical Absorption Intensities of Rare-Earth Ions. *Phys. Rev.* **1962,** *127,* 750-761.

(60) Ofelt, G. S., Intensities of Crystal Spectra of Rare-Earth Ions. *J. Chem. Phys.* **1962,** *37,* 511-520.

Table 1: Dopant concentration added in solution and actual concentration in solid measured by TXRF

Sample	Europium in solution (mol %)	Europium in solid (mol %)
CEEU0.2	0.3	0.2
CEEU0.8	1	0.8
CEEU1.5	2	1.5
CEEU3.9	5	3.90
CEEU7.6	10	7.62
CEEU13.9	20	13.94
CEEU19.2	30	19.23
CEEU24.6	40	24.58
CEEU29.2	50	29.23

Table 2: Variation of particle size, band gap, Ce^{3+} ions concentration, lattice parameter and strain measurements with different europium concentrations and annealed ceria nanoparticles

Sample	Europium in solid sample (mol %)	Annealing temp. (° C)	Particle size (nm)	Band gap (eV)	% Ce^{3+}	Lattice parameter a (Å)	Strain (x10^{-3})
CEEU0	Undoped		8.77	3.34	0	5.4201	1.65
CEEU0.2	0.2		8.19	3.26	-	5.4195	1.68
CEEU0.8	0.8		7.76	3.21	-	5.4188	1.75
CEEU1.5	1.5		6.99	3.17	1	5.4171	1.91
CEEU3.9	3.9		5.2	3.13	4	5.4289	3.26
CEEU7.6	7.6		5.07	3.11	7	5.4301	3.49
CEEU13.9	13.9		4.83	3.07	14	5.4328	3.98
CEEU19.2	19.2		4.8	3.05	19	5.4332	4.06
CEEU24.6	24.6		4.8	3.03	24	5.4335	4.58
CEEU29.2	29.2		4.8	3.02	29	5.4338	5.07
CEEU7.6-500	7.6	500	5.31	3.12	5	5.4270	2.89
CEEU7.6-700	7.6	700	9.48	3.17	4	5.4249	2.29
CEEU7.6-900	7.6	900	27.23	3.30	4	5.4211	1.81
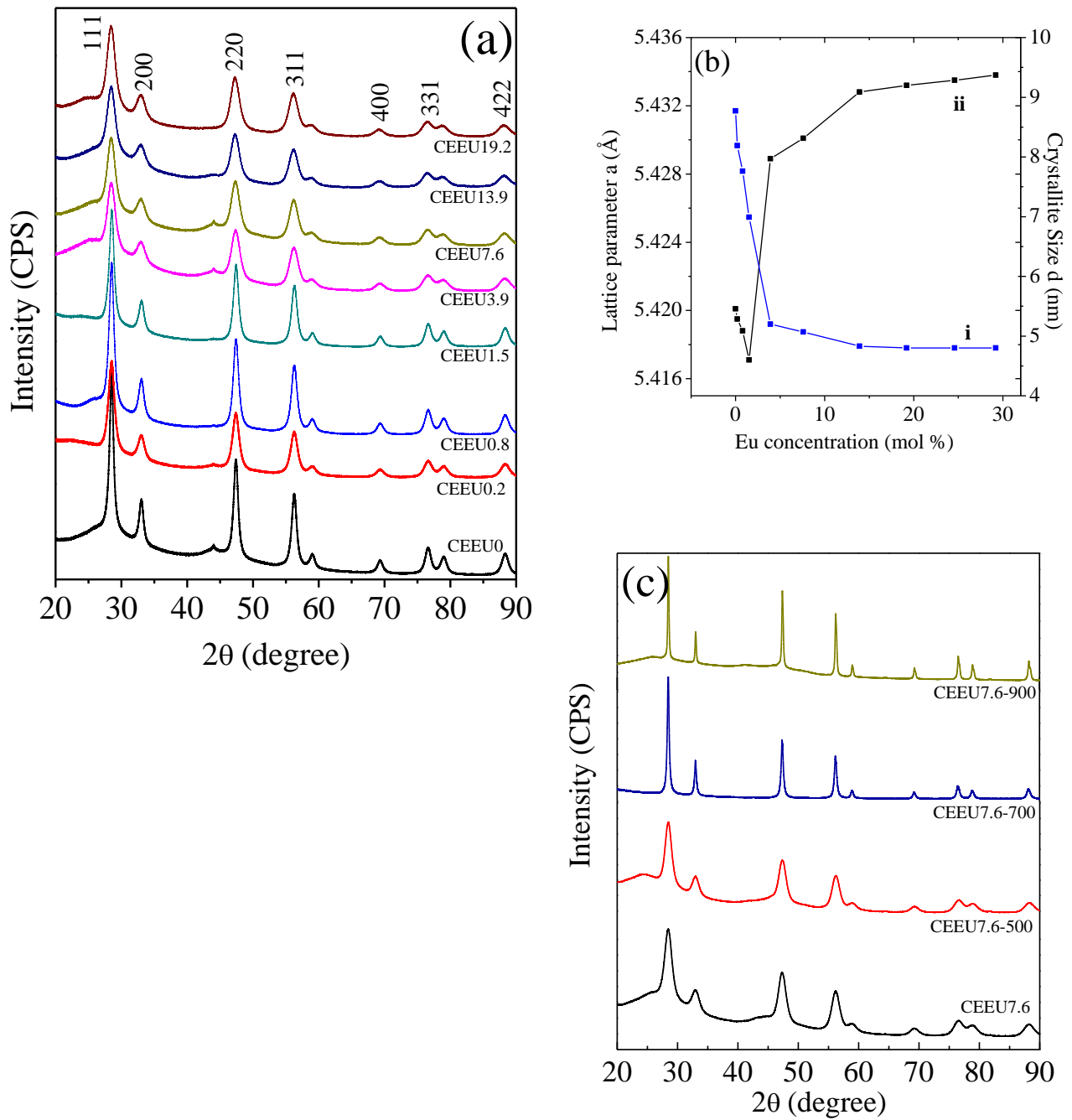
Figure 1. (a) XRD spectra of undoped and Europium doped cerium oxide samples (b) Crystallite size [i] and lattice parameter [ii] variation with increase in Europium concentration. (c) XRD spectra of CEEU7.6 sample annealed at different temperatures.
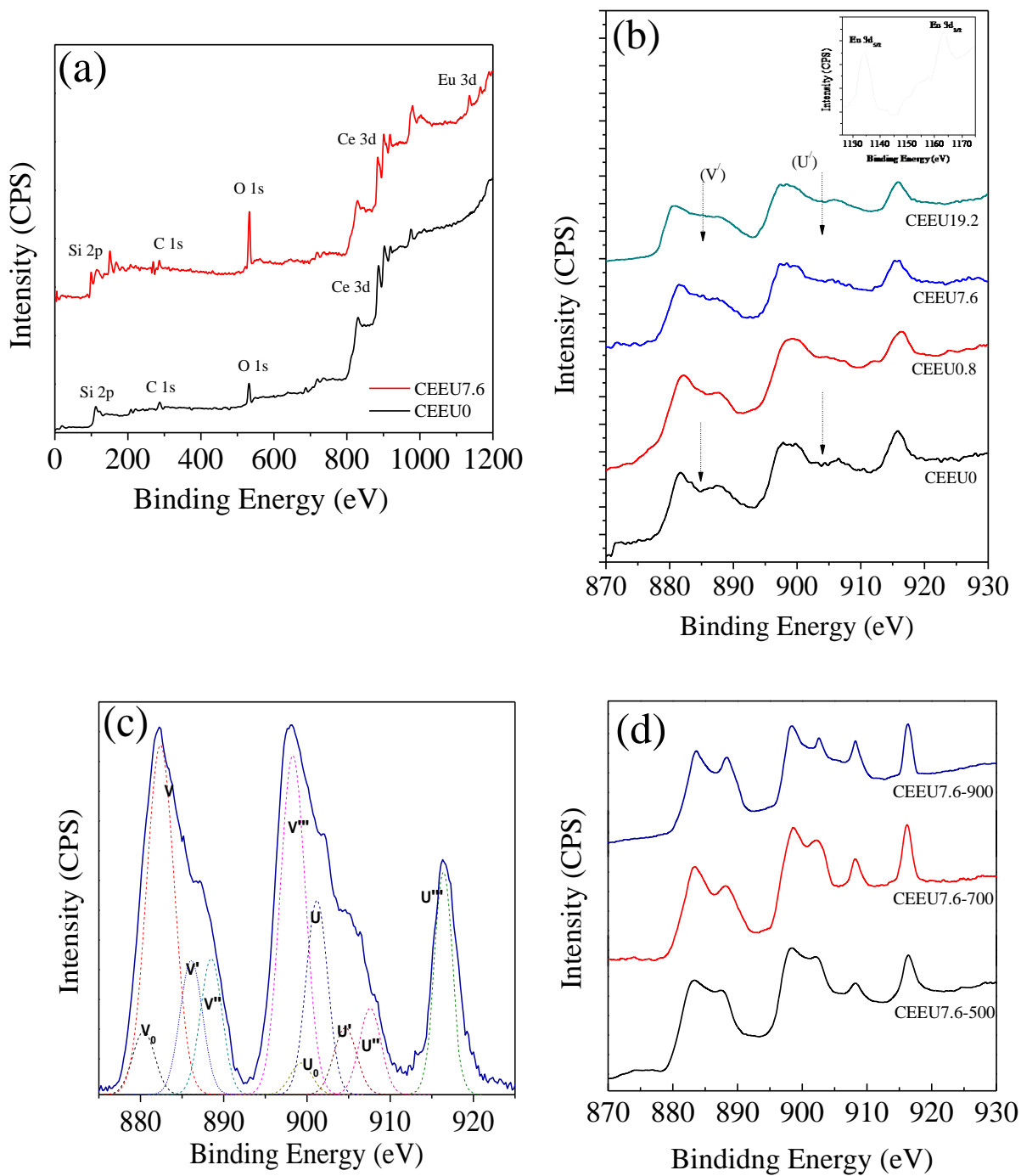
Figure 2. (a) XPS survey spectra of CEEU0 and CEEU7.6 samples. (b) Ce 3d spectra of CEEU0, CEEU0.8, CEEU7.6 and CEEU19.2 samples. Inset shows the Eu 3d spectrum of CEEU7.6 (c) Cerium 3d spectra of CEEU7.6 (d) Ce 3d spectra of CEEU7.6 sample annealed at various temperatures.
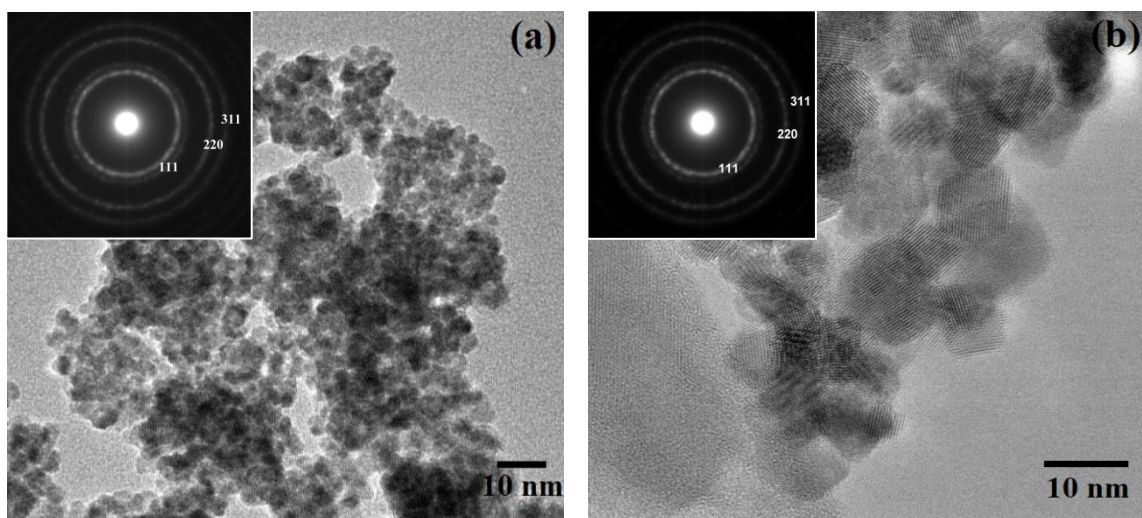
Figure 3. TEM images of undoped and europium doped CeO$_2$ nanoparticles (a) CEEU0 (b) CEEU0.8 (c) CEEU7.6 (d) CEEU19.2. (Inset shows corresponding SAED)
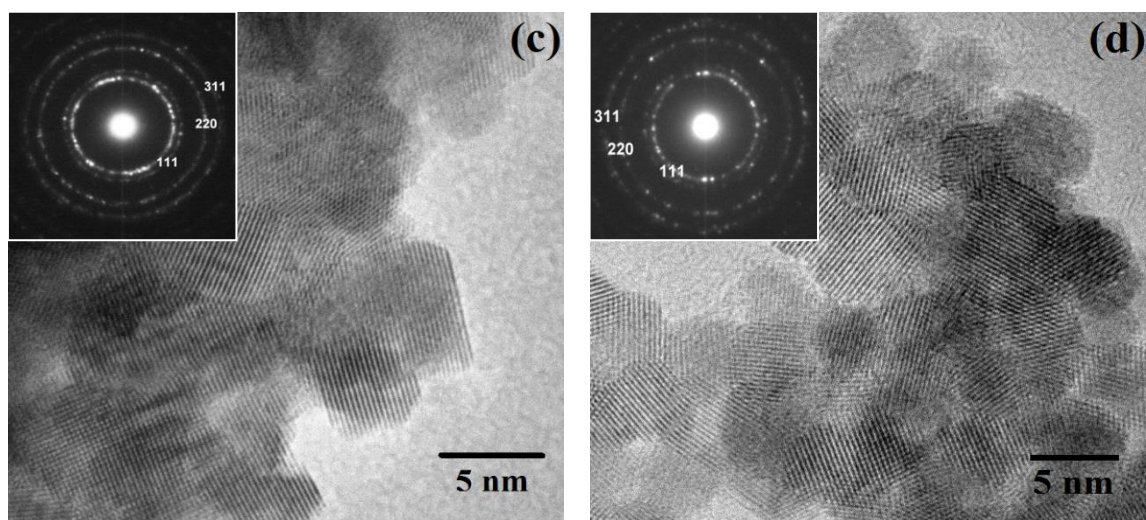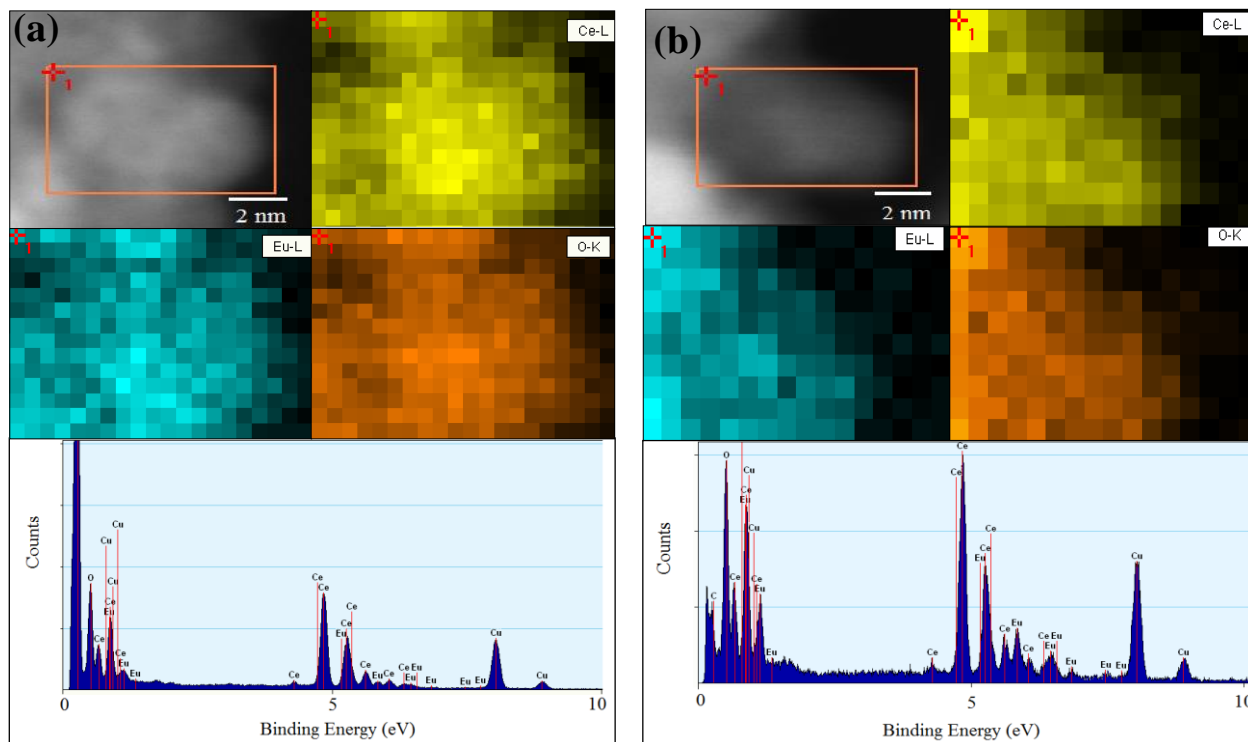
Figure 4. Ce-L, Eu-L, O-K mapping of europium doped CeO_2 and respective EDX spectrum recorded on a single nanoparticle in the marked box (a) CEEU7.6 (b) CEEU19.2.
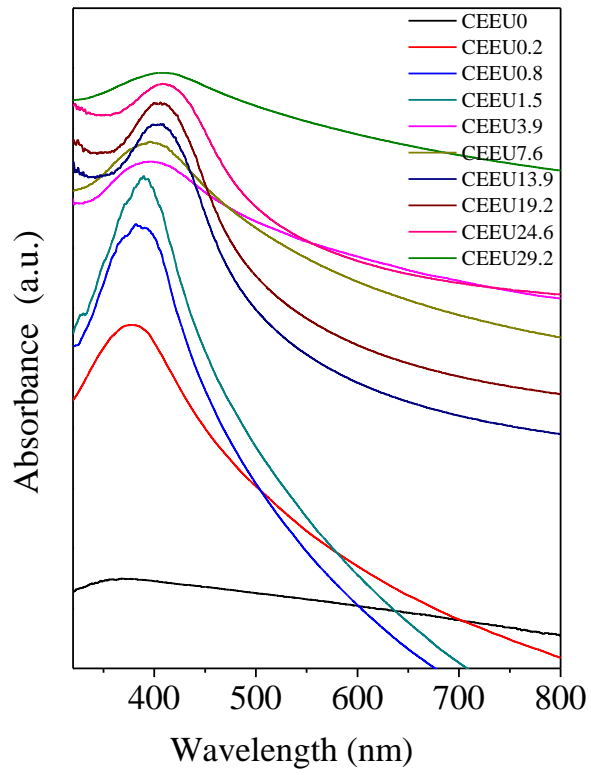
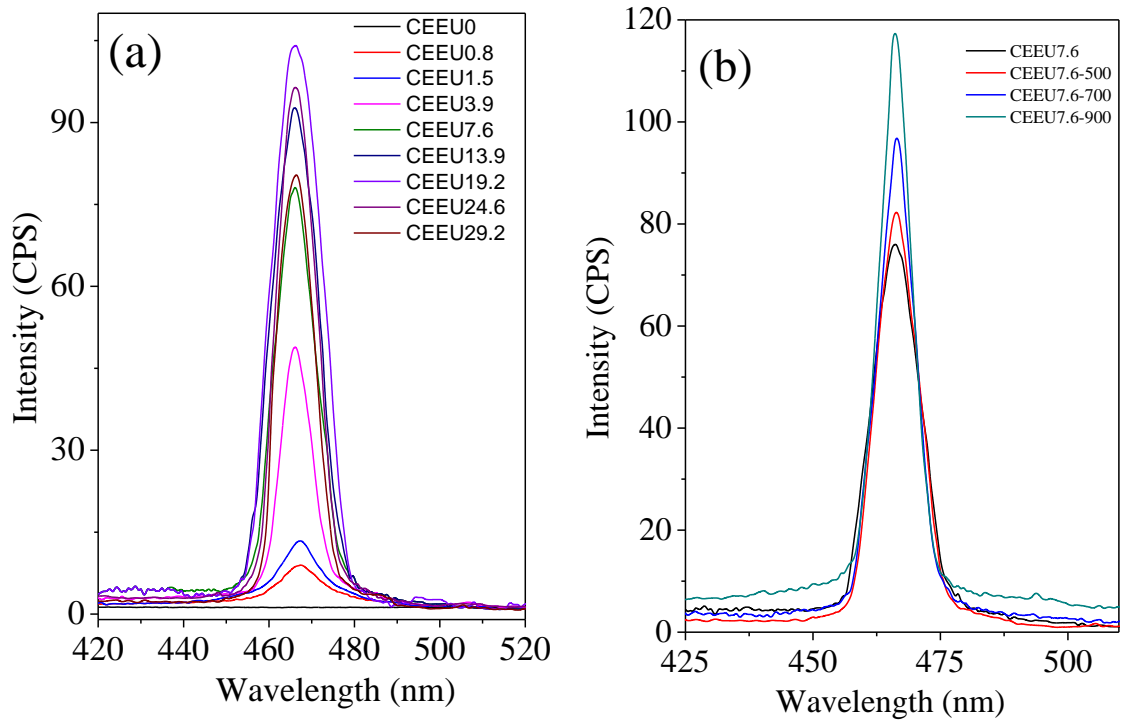**Figure 5.** UV-Vis absorption spectra of undoped and Europium doped CeO$_2$ nanoparticles.

Figure 6. Excitation spectra with emission at

608 nm for (a) as prepared samples (b) CEEU7.6 sample annealed at various temperatures.
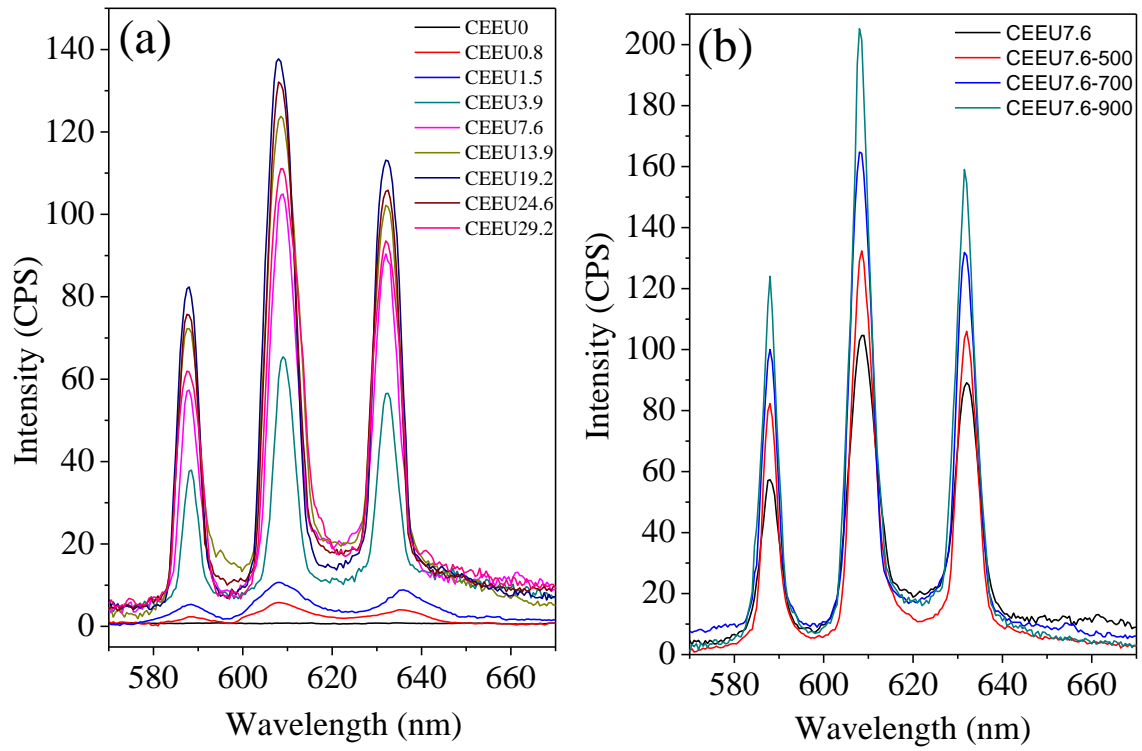
Figure 7. Emission spectra with excitation at 466 nm for (a) as-prepared samples (b) CEEU7.6 sample annealed at various temperatures.